Carrier Phase Estimation Through the Rotation Algorithm for 64-QAM Optical Systems

Carrier Phase Estimation through the Rotation Algorithm for 64-QAM Optical Systems

S. M. Bilal, Student Member, IEEE, G. Bosco, Senior Member, IEEE, J. Cheng, Alan Pak Tao Lau, C. Lu

***Abstract*—A novel low-complexity two-stage digital feed-forward carrier phase estimation (CPE) algorithm based on the rotation of constellation points to remove phase modulation for a 64-ary quadrature amplitude modulation (QAM) system is proposed and analyzed both experimentally and through numerical simulations. The first stage is composed of a Viterbi&Viterbi block, based on either the standard quadrature phase shift keying (QPSK) partitioning algorithm using only Class-1 symbols or a modified QPSK partitioning scheme utilizing both Class-1 and outer most triangle-edge (TE) symbols. The second stage applies the Viterbi&Viterbi algorithm after the removal of phase modulation through rotation of constellation points. Comparison of the proposed scheme with constellation transformation (CT), blind phase search (BPS) and BPS+MLE (maximum likelihood estimation) algorithm is also shown. For an OSNR penalty of 1 dB at bit error rate (BER) of 10^{-2}, the proposed scheme can tolerate a linewidth times symbol duration product ($\Delta\nu \cdot T_s$) equal to 3.7×10^{-5}, making it possible to operate 32-Gbaud optical 64-QAM systems with current commercial tunable lasers.**

***Index Terms*—Bit error rate (BER), carrier phase recovery, Viterbi & Viterbi algorithm, quadrature amplitude modulation (QAM), triangle edge (TE) symbols, rotation algorithm (RA)**

I. Introduction

In the past few years, coherent optical detection has emerged as a compelling approach for enhanced data rates. Combined with multilevel M-ary QAM formats, coherent optical detection is considered to be the best candidate for future high-capacity 100 and 400 Gbps wavelength-division multiplexing (WDM) systems [1]–[5]. However, a critical part of coherent optical communication systems is the phase sensitive coherent receiver whose performance is limited by the phase noise that exists on the recovered data samples [6]. Major source of phase noise is the finite linewidth of both transmitter (Tx) laser and receiver (Rx) local oscillator [7], [8]. Amplified Spontaneous Emission (ASE) creating nonlinear phase noise that interacts with the nonlinear Kerr effect, can also add in the phase noise of recovered data signal [9]. This phase noise causes distortion and hence random rotation of the received constellation points [10]. As a consequence, design of efficient carrier phase estimation (CPE) algorithms has become very important, especially while implementing high-order modulation formats.

S. M. Bilal and G. Bosco are with Dipartimento di Elettronica, Politecnico di Torino, Italy (e-mail: bilalsyedm@gmail.com). A. P. T. Lau and C. Lu are with the Photonics Research Center, The Hong Kong Polytechnic University, Hong Kong, China. J. Cheng is with the Next Generation Internet Access National Engineering Lab, Huazhong University of Science and Technology, Wuhan, China.

Up till now, various feed-forward CPE algorithms have been proposed, the most popular being based on either QPSK partitioning [11]–[16] or blind phase search (BPS) [17] algorithms. BPS algorithms, originally introduced for more general synchronous communication systems [18], [19], have very high linewidth tolerance but they come at an expense of additional computational complexity [17]. This complexity however, can be lowered by reducing the number of *'test phase angles'* [20], [21]. QPSK partitioning schemes on the other hand, are derived from the classical Viterbi and Viterbi (V&V) phase estimation approach [22]. When applied to high-order modulation formats, these algorithms require dedicated symbols and adhoc amplitude discrimination for carrier phase estimation. However, V&V algorithms are simpler to implement and have much smaller computational complexity.

In this paper we propose and analyze both experimentally and through numerical simulations, a two-stage low complexity algorithm to compensate for phase noise in 64-QAM systems. The technique is an extension to 64-QAM of a similar approach presented in [23] for 16-QAM. The remainder of the paper is organized as follows. In Section II, an overview of the conventional CPE technique based on V&V is given. In Section III, a modification in this scheme to include triangle edge (TE) symbols is described while the rotation algorithm, that serves as a second stage for both the techniques, is explained in Section IV. Simulation setup and results are presented in Section V whereas experimental setup and results are reported in Section VI. Section VII describes the complexity computations of different schemes along with their analysis. We conclude our work in Section VIII.

II. Conventional CPE Techniques Overview

Fig. 1 shows the constellation plot of a 64-QAM system affected by Additive Gaussian Noise (AGN), as for instance the Amplified Spontaneous Emission (ASE) noise introduced by optical amplifiers. Rings C_1 to C_{10} in the figure indicate different thresholds for separating symbols of different amplitudes. One possible approach is to perform phase estimation using the conventional V&V algorithm considering only Class-1 symbols, i.e. symbols that lie at modulation angles of $\pi/4 + m \cdot \pi/2$ ($m = 0 \ldots 3$) and indicated by rings C_1, C_3, C_7 and C_{10}. These symbols are highlighted using red dashed circles in Fig. 1. Note that only 12 out of the 16 symbols lying at the vertices of squares are used. The symbols in the ring C_7 are neglected as their modulus is very similar to the symbols in the ring C_6, making their identification critical, which hence could lead to additional errors. The block diagram

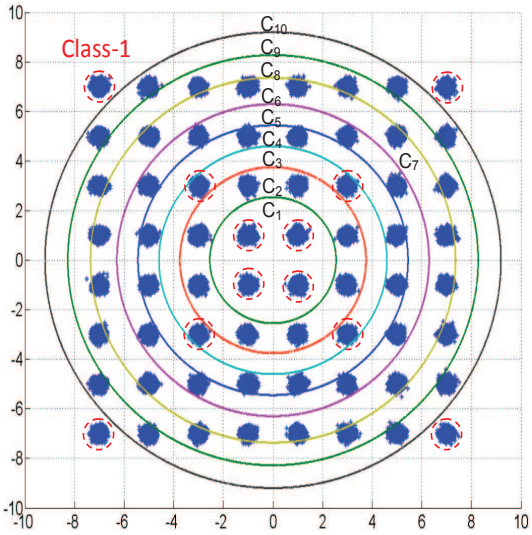

Fig. 1. 64-QAM Constellation with different thresholds for separating symbols of different amplitudes. Class-1 symbols used in the first Viterbi&Viterbi stage are highlighted by red dashed circles.

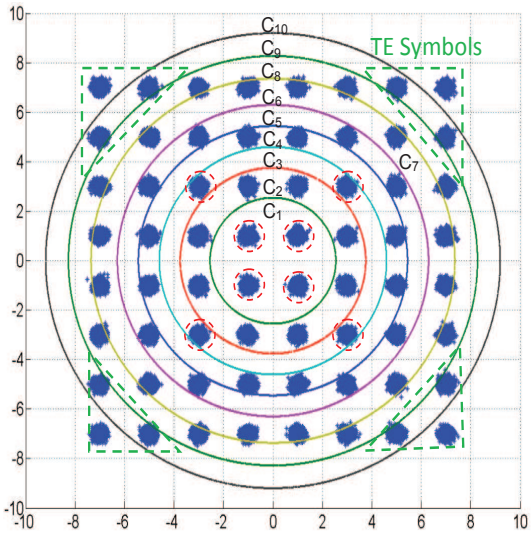

Fig. 2. 64-QAM Constellation with different thresholds for separating symbols of different amplitudes. Symbols used in the first Viterbi&Viterbi stage are highlighted by red dashed circles & green triangles .

of the algorithm is shown in Fig. 3a. The complex samples are raised to the 4-th power to remove the phase modulation. To increase the accuracy of the estimate, a moving average with a uniform centered window of length N_1 symbols is performed. By finding the angle of the complex sum vector, a phase error estimate is obtained for this block. The complex samples are normalized before adding them up for phase estimation:

$$\varphi_{n,(est,class1)} = \frac{1}{4}\arg \sum_{k=n-\frac{N_1}{2}+1}^{n+\frac{N_1}{2}} \frac{X_k^4}{|X_k^4|} \qquad (1)$$

Whenever a symbol is received that does not belong to Class-1, a 'zero' is inserted at its place in the vector of samples used for phase estimation in Eq. (1), .i.e. that particular symbol does not give any contribution to the phase estimation but the length of the averaging window N_1 includes also non-Class-1 symbols.

Since only a small percentage of all the symbols is used ($\approx 19\%$), phase estimation obtained by using these symbols is not suitable to track fast phase variations: it is potentially able to compensate for a laser linewidth which is approximately 1/5 of the linewidth that could be compensated for if all 64 symbols were used.

III. Modified V&V Algorithm (V&V*)

In [12]–[14] and [24] we have shown that a better phase noise tolerance can be achieved, if it is possible to increase the number of symbols that took part in the phase estimate. The scheme presented in [13] and [24] makes a carrier phase estimation by raising to the power of four not only Class-1 symbols, but also symbols which lie at an angle close but not exactly equal to $\pi/4 + m \cdot \pi/2$ ($m = 0 \ldots 3$). In this way, the number of symbols that take part in the phase estimate is increased and a better phase noise tolerance is achieved, provided that the angle of deviation of the new symbols with respect to Class-1 symbols is sufficiently small.

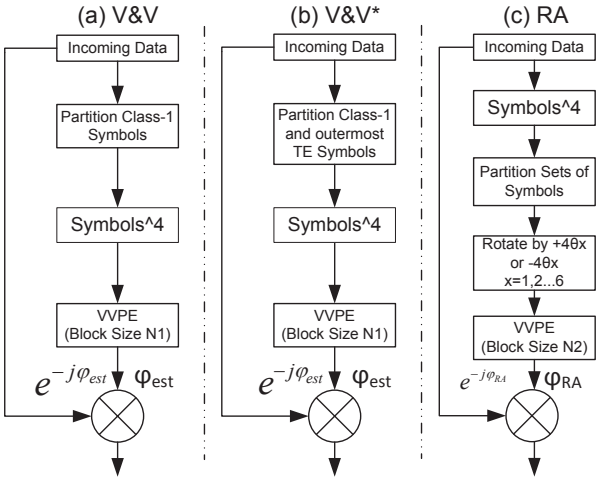

Fig. 3. Block diagrams of the elementary CPE stages

Hence for this estimator Class-1 symbols of the inner 16-QAM along with the outermost triangle edge (TE) symbols of the 64-QAM constellation are selected (Fig. 2). In Fig. 2 TE and Class-1 symbols are shown by green dashed triangles and red dashed circles, respectively. The block diagram is shown in Fig. 3b, where phase estimation is obtained by using conventional VVPE algorithm by raising the symbols to the power of 4 (see eq. (1)). Averaging is performed over N_1 symbols, while using a uniform filter with centered window. Since the triangle edge symbols lie at an angle of $\pm 9.5^\circ$ from $m \cdot \pi/4 (m = 1, 3, 5, 7)$, raising them to the power of 4 will approximately reduce them to the single phase vectors and if the averaging window is sufficiently long this $\pm 9.5^\circ$ error is averaged out and the estimation of phase noise is only marginally affected by these errors. We have named this scheme as V&V* algorithm.

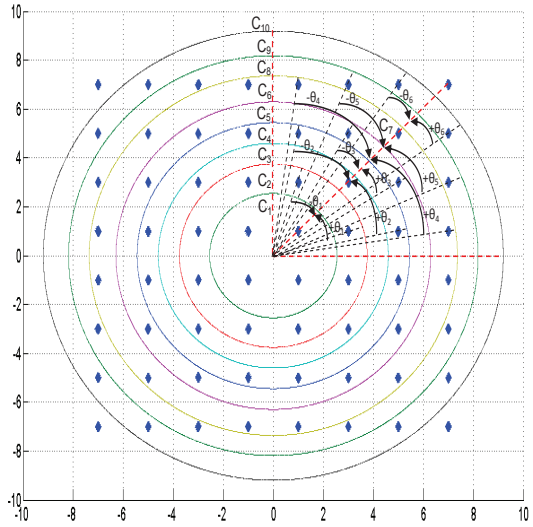

Fig. 4. 64-QAM constellation showing all the rings and their rotation angles from $\pi/4$

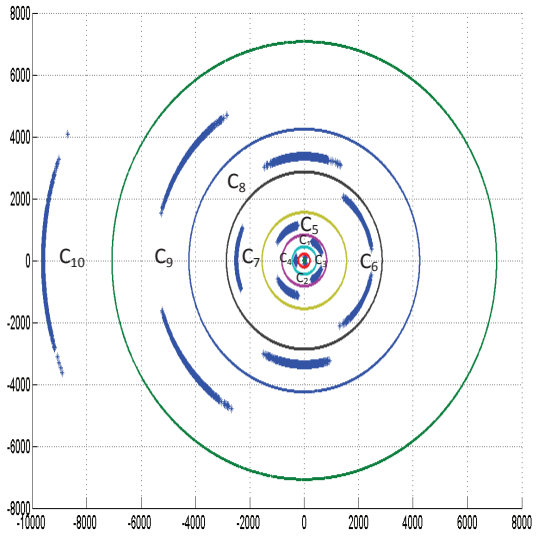

Fig. 6. Plot after raising the 64-QAM constellation to 4th power

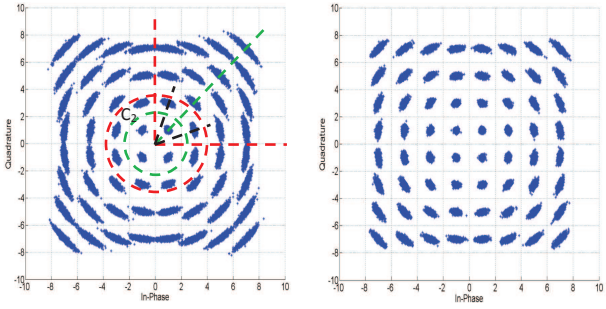

Fig. 5. 64-QAM constellation after coarse (left) and fine (right) carrier phase estimation

IV. Rotation Algorithm (RA)

After getting a coarse phase estimate by applying V&V or V&V* algorithm, a fine estimate can then be obtained by using the rotation algorithm (RA) that will be described in the following.

As can be seen in Fig. 4, 64-QAM constellation symbols can be divided into ten sub classes, based on their amplitude. Fig. 4 shows the different thresholds for separating symbols of different amplitudes. Symbols in the rings C_1, C_3, C_7 and C_{10} are the QPSK partitioned symbols that lie at modulation angles of $\pi/4 + m \cdot \pi/2$ $(m = 0 \ldots 3)$. As previously mentioned, symbols in ring C_7 are not used for a phase noise estimation in the 1st stage, as their modulus is very similar to the symbols in ring C_6 and hence can result in additional errors. Symbols in the rings C_2, C_4, C_5 C_6, C_8, and C_9 can be categorized into two sets of QPSK symbols with phase rotations $\pm\theta_1 = \pi/4 - \tan^{-1}(1/3)$, $\pm\theta_2 = \pi/4 - \tan^{-1}(1/5)$, $\pm\theta_3 = \pi/4 - \tan^{-1}(3/5)$, $\pm\theta_4 = \pi/4 - \tan^{-1}(1/7)$, $\pm\theta_5 = \pi/4 - \tan^{-1}(3/7)$ and $\pm\theta_6 = \pi/4 - \tan^{-1}(5/7)$, respectively, with respect to the symbols lying in the rings C_1, C_3, C_7 or C_{10} (Fig. 4).

Fig. 5 shows a 64-QAM constellation plot after getting a coarse (left side) and fine (right side) carrier phase estimation with 64-ideal points shown as short arcs, due to the phase noise. An example is shown in Fig. 5 (left side), considering symbols in ring C_2, first quadrant: if the residual phase noise is not very large, symbols in this ring will not cross the boundary shown by the green dashed line. The same will be true for the symbols in rings C_4, C_5 C_6, C_8, and C_9. If the residual phase noise after the coarse carrier phase estimation is sufficiently small not to cross the boundaries between the symbols in corresponding rings, these symbols can be properly rotated by $\pm\theta_x$ $(x = 1 \ldots 6)$, respectively, in order to make them fall at an angle equal to $\pi/4 + m \cdot \pi/2$ $(m = 0 \ldots 3)$. After that, all the symbols can be raised to the power of 4 to remove the phase modulation. However, there will be some additional computational complexity to distinguish the symbols that are either at an angle of $+\theta_x$ or $-\theta_x$.

To minimize this complexity, we have first raised the symbols to the power of 4 before applying this RA technique (Fig. 3(c)).

$$Z_k = Y_k^4 \tag{2}$$

where Y_k are the rotated data samples after 1st stage of carrier phase recovery. Constellation plot after the 4th power operation is shown in Fig. 6 where symbols belonging to all the rings (C_1 to C_{10}), are collapsed down to unique positions. Having distinct thresholds, all the symbols now can be easily separated. Since symbols in the rings C_6 and C_7 lie inside the same threshold circle, an additional comparator will be needed to separate them from each other. **This only requires setting up a threshold around zero for real values of C_6 and C_7 symbols (Fig. 6).** Phase modulation of the rings C_1, C_3, C_7 and C_{10} is removed while the phase modulation of the rings C_2, C_4, C_5 C_6, C_8, and C_9 can be removed by [23]:

$$RA_y = C_y \times \exp(4j\theta_x \times \mathrm{sgn}(Im(C_y))) \tag{3}$$

where y= $2, 4, 5, 6, 8, 9$, $x = 1, 2, ...6$, $sgn(.)$ is the $'signum'$ function and $Im(.)$ is the imaginary part of the complex valued symbol. After this rotation, phase modulation of C_2, C_4, C_5 C_6, C_8, and C_9 rings is also removed as shown

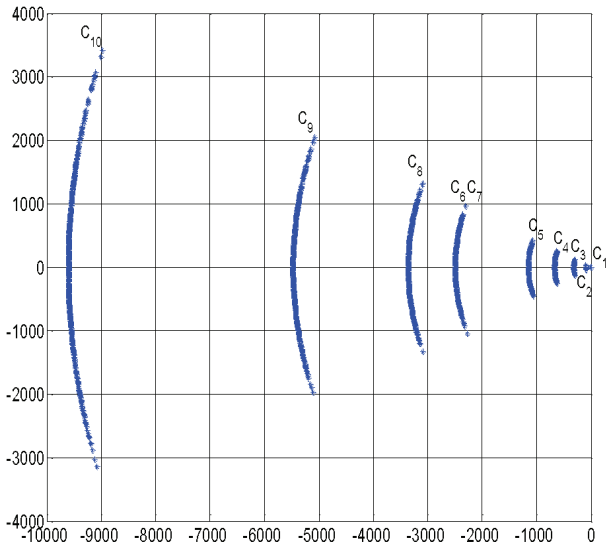

Fig. 7. 64-QAM constellation after fourth power and rotation operation

in Fig. 7. Since the modulus of the rings C_6 and C_7 is almost the same, their constellation after this rotation would also be the same (Fig. 7). After this, the conventional V&V algorithm is applied to get a fine carrier phase estimation but the symbols now will not be raised to the 4th power, as the 4th power operation has already been applied:

$$\varphi_{n(RA)} = \frac{1}{4}\arg \sum_{k=n-\frac{N_2}{2}+1}^{n+\frac{N_2}{2}} \frac{X_k}{|X_k|} \tag{4}$$

N_2 refers to the averaging performed over symbols using a uniform filter with centered window.

As previously mentioned, phase noise should be small enough so that the rotation angles $\pm\theta_x$ ($x = 1 \dots 6$) are in the range $[0, \pm\pi/4]$. In the presence of frequency offset or large residual phase noise, the constellation points at $+\theta_x$ and $-\theta_x$ will rotate and cross the boundary (green dashed line), shown in Fig. 5 (left side) for ring C_2. The same will happen to the other rings C_4, C_5 C_6, C_8, and C_9. It means that, after raising the symbols to the power of 4, some of the constellation points would be transformed in the wrong direction, resulting in an incorrect phase estimate. It is for this reason that, RA serves as a 2nd stage for phase noise compensation after frequency offset compensation and coarse carrier phase estimation.

V. Simulation Setup and Results

In this section we compare by simulation, the performance of the proposed two-stage RA algorithm with CT [24], [25], BPS [17] and BPS+MLE [26] schemes.

The equalized signal samples, affected by both additive Gaussian noise and phase noise, can be written as:

$$y_k = x_k e^{j\theta_k} + n_k \tag{5}$$

x_k is the data symbol that belongs to the set $(\pm a \pm jb)$, a, $b \in \{1, 3, 5, 7\}$ and n_k is the additive white Gaussian noise (AWGN), which models for instance the ASE noise introduced

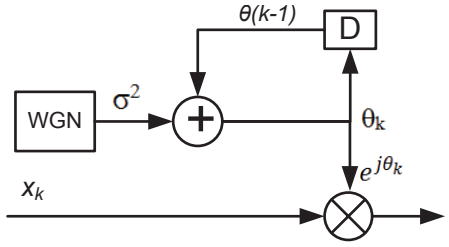

Fig. 8. Phase Noise Model

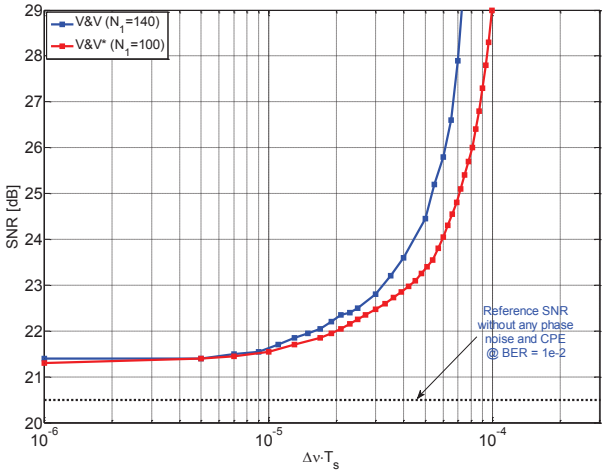

Fig. 9. A comparison of SNR vs linewidth times symbol duration ($\Delta\nu \cdot T_s$) for phase error estimate obtained by using V&V and V&V* algorithms

by optical amplifiers. θ_k is the laser phase noise and is modeled as a Wiener process [17], as shown in Fig. 8:

$$\theta_k = \sum_{i=-\infty}^{k} v_i \tag{6}$$

v_i's are independent and identically distributed Gaussian random variables with zero mean and variance

$$\sigma_f^2 = 2\pi\Delta\nu \cdot T_s \tag{7}$$

$\Delta\nu$ is the laser linewidth and T_s is the symbol period.

In our simulations, each 64-QAM symbol was generated combining 6 different PRBS sequences of length equal to $2^{15}-1$ and the BER was evaluated by error counting over ~100,000 symbols. Fig. 9 shows the performance comparison between the two single-stage algorithms V&V and V&V* in terms of SNR (defined over a bandwidth equal to the symbol-rate $R_s = 1/T_s$) required to obtain a target BER equal to 10^{-2} as a function of the product $\Delta\nu \cdot T_s$.

Fig. 10 shows the performance comparison of different analyzed algorithms. The values of N_1, N_2, and M reported in the legend indicate the lengths of averaging windows and test phase angles, respectively, used in the corresponding algorithms, optimized by maximizing the linewidth tolerance at 1-dB penalty [14], [17]. For our simulations we have chosen the target BER=10^{-2} so that the system can tolerate a 1-dB SNR penalty due to phase noise without exceeding the FEC threshold, which is assumed to be 2×10^{-2}, as granted by

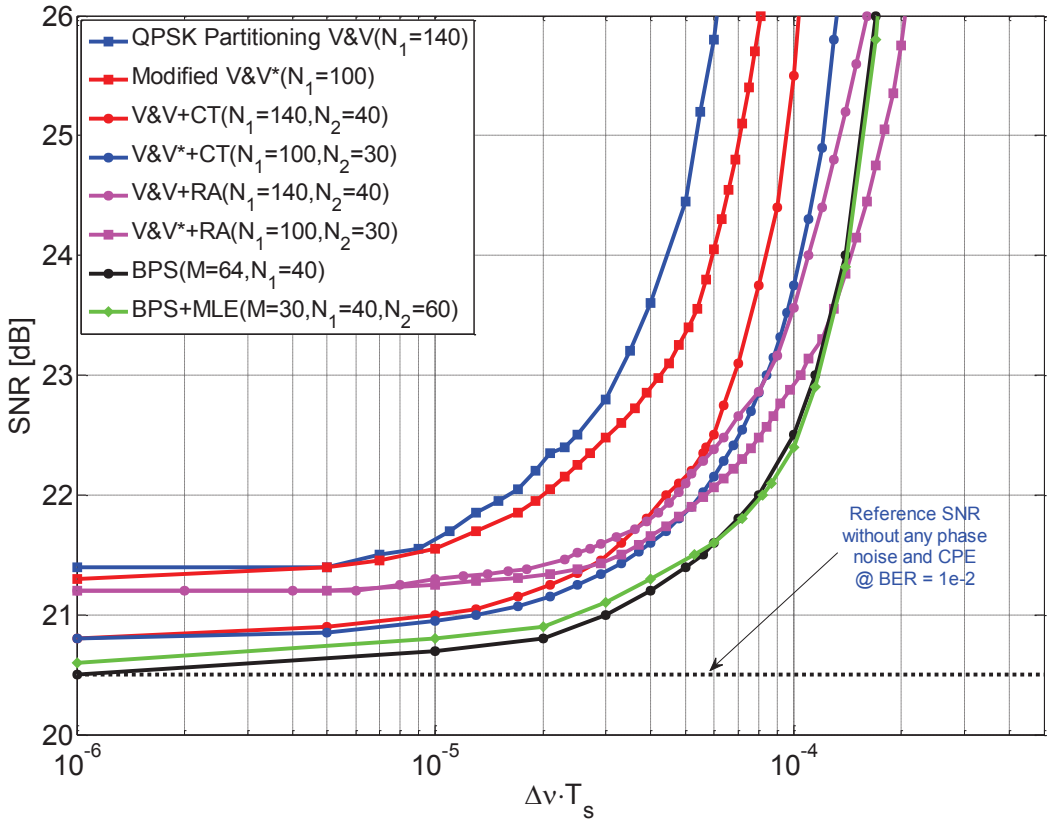

Fig. 10. SNR vs linewidth times symbol duration ($\Delta\nu \cdot T_s$) productat BER=10^{-2} for different CPE schemes

current state-of-the-art soft FEC codes with 20% overhead [27]. Table I shows the linewidth tolerances (i.e linewidth times symbol duration products) of different schemes at 1-dB penalty with respect to the SNR needed to achieve BER=10^{-2} in the absence of phase noise (i.e. ≈ 20.5 dB).

No cycle slip was detected in our simulations. However, considering lower SNR values and larger line-widths, cycle slips could indeed occur, and could be compensated by using differential encoding. Using angle differential encoding [28] it was observed that the SNR penalty will increase by 0.7~0.8 dB to achieve the same linewidth tolerances ($\Delta\nu \cdot T_s$) at 1 dB penalty with respect to the reference SNR (see Fig. 10) for all the schemes.

From Fig. 10 it is evident that the sensitivity of RA is not as good as CT or BPS but the stability at high phase noise values is even better than BPS. This is perhaps because in CT all the 64 symbols are collapsed down to 4 constellation points, loosing their individual identity whereas in RA all the symbols just undergo a rotation, hence maintaining their individualness. However, at 1 dB penalty the tolerance of RA is the same as that of CT.

VI. Experimental Setup and Results

The experimental setup is shown in Fig. 11 An external cavity laser (ECL) with a linewidth of 100 kHz and wavelength 1553.32 nm is modulated by an integrated IQ modulator. The I and Q branches of the IQ modulator are driven by two 20-Gbaud 8-level electrical signals in order to generate a 64-QAM signal. The dual-polarization (DP) 64-QAM signal is generated by using a polarization multiplexing emulator. By loading different amounts of ASE noise, the optical-signal-to-noise-ratio (OSNR) values were varied between 25 and 37 dB. At the receiver side, an optical band pass filter (OBPF) with bandwidth 0.6nm is used for filtering the out-band noise. The received signal is coherently detected by an integrated coherent receiver with a local oscillator (ECL, with line-width 100 kHz). The detected signal is sampled by a 50GS/s real-time sampling scope. The captured data is processed offline using following DSP algorithms:

1) Deskew and orthogonalization.
2) Digital filtering with (0.6/Ts) 3-dB bandwidth.
3) Resampling to 2 samples/symbol.
4) Chromatic dispersion (CD) compensation.
5) Clock recovery.
6) 13 taps, Ts/2-spaced constant modulus algorithm (CMA) for pre-convergence followed by radius-directed algorithm (RDA) for steadystate equalization.
7) Frequency offset compensation and carrier phase estimation (CPE) using techniques described in this paper.
8) 801-taps least mean square (LMS) filter for performance optimization followed by standard symbol detection and BER calculation.

Such long 801 taps LMS filter is mainly used for compensating the inter-symbol-interference (ISI) induced by the reflections of radio frequency (RF) signals between high frequency electrical components such as connectors and 3bit digital-to-analog converter (DAC) that is used for the 64-QAM signal generation. This reflection is due to

1st Stage	2nd Stage	LW Tolerance ($\Delta\nu \cdot T_s$)	Equivalent LW @ 20 Gbaud	Equivalent LW @ 32 Gbaud
V&V		8.0×10^{-6}	0.16 MHz	0.25 MHz
V&V*		1.0×10^{-5}	0.20 MHz	0.32 MHz
V&V	CT	3.0×10^{-5}	0.60 MHz	0.96 MHz
V&V*	CT	3.7×10^{-5}	0.74 MHz	1.18 MHz
V&V	RA	3.0×10^{-5}	0.60 MHz	0.96 MHz
V&V*	RA	3.7×10^{-5}	0.74 MHz	1.18 MHz
BPS		5.7×10^{-5}	1.14 MHz	1.82 MHz
BPS	MLE	5.4×10^{-5}	1.08 MHz	1.72 MHz

TABLE I
LASER PHASE NOISE TOLERANCES

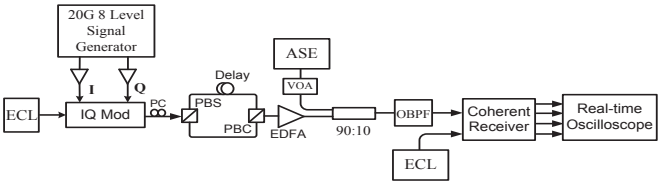

Fig. 11. Experimental setup for 240Gb/s (20Gbaud) DP-64QAM back-to-back system

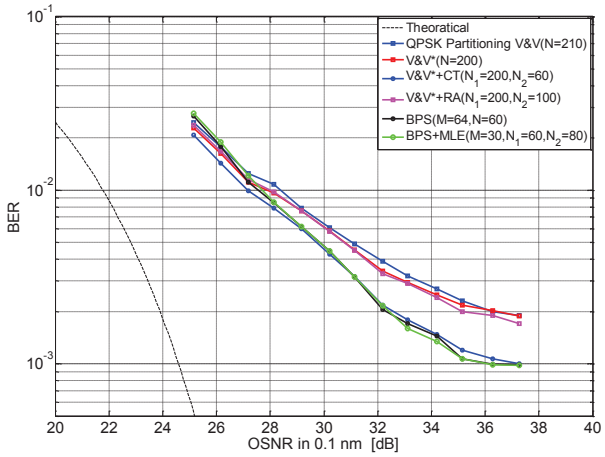

Fig. 12. BER vs OSNR performance (back to back) for different CPE algorithms

the RF impedance mismatching. With carefully building up the transmitter, we can shorten the length of the LMS taps in the receiver. The presence of this filter however does not affect the performance comparison of the various CPE techniques. Fig. 12 shows the back to back performance of different analyzed algorithms. For a 20 Gbaud system with $\Delta\nu \cdot T_s$=5.0×10^{-5}, corresponding to a combined Transmitter laser+LO linewidth of 200 kHz, the optimum block lengths and test phase angles of different schemes are reported in the legend of Fig. 12.

From Fig. 12 it can be seen that the performance of RA is the almost same as that of V&V* and slightly worse than CT and BPS. This is because the experimental analysis is for very small value of $\Delta\nu \cdot T_s(5.0 \times 10^{-6})$ which corresponds to a combined Transmitter laser+LO linewidth of 200 kHz only. For large values of $\Delta\nu \cdot T_s$ or Transmitter laser+LO linewidths, it is possible that RA scheme might have same or even better performance than CT or BPS.

VII. COMPLEXITY COMPUTATIONS AND ANALYSIS

The complexity evaluations reported in Table II are referred to the processing of a single polarization with phase unwrapping and optimum implementation. For example, by doing some mathematical computations it can be shown that the $4th$ power of a complex value needs only 6 real multipliers and 2 adders instead of 8 real multipliers and 4 adders. The complexity computations however do not consider the normaliztion factor. Complexity analysis for BPS and BPS+MLE is also focused on optimization of multiplications and is not implemented using a CORDIC (coordinate rotation digital computer) algorithm [17]. Complexity of RA is almost the same as that of CT and almost 9 times less than that of BPS. Complexity of BPS+MLE is almost 2.5 times less than that of BPS.

This technique could also be extended to a 8-QAM, 32-QAM, 128-QAM or 256-QAM systems. Knowing the rotation angles of all non Class-1 symbols, they can be rotated/de-rotated to make them fall at an angle of $\pi/4 + m \cdot \pi/2$ ($m = 0 \ldots 3$). Then the algorithm proposed in this manuscript can be used to get a fine carrier phase estimation.

VIII. CONCLUSION

In this paper, we have analyzed through both simulations and experiments the performance of a two-stage phase noise tolerant feed forward carrier phase estimation algorithm for a 64-QAM system. The first stage makes a coarse carrier phase estimation by employing either a simple QPSK partitioning algorithm (V&V) or a modified QPSK partitioning scheme (V&V*). The second stage makes a fine estimate by removing the phase modulation through rotation of the symbols by certain degrees. Comparison of the proposed RA scheme with CT, BPS and BPS+MLE scheme is also shown. At 1-dB penalty and target BER of 10^{-2} the proposed technique can tolerate a times symbol duration product ($\Delta\nu \cdot T_s$) equal to 3.7×10^{-5}. So at the industry-standard symbol rate of 32 GBaud, the proposed technique can tolerate a combined laser

CPE	Real Multipliers	Real Adders	Comparators	Look-Up Tables	Decisions
V&V	$8N_1$	$3N_1$+2	$4N_1$+2	1	N_1
V&V*	$8N_1$	$3N_1$+2	$4N_1$+2	1	N_1
V&V+CT	$8N_1$+$6N_2$	$3N_1$+$3N_2$+30	$4N_1$+7	2	N_2
V&V*+CT	$8N_1$+$6N_2$	$3N_1$+$3N_2$+30	$4N_1$+7	2	N_2
V&V+RA	$8N_1$+$6N_2$+36	$3N_1$+$3N_2$+4	$4N_1$+13	3	N_2
V&V*+RA	$8N_1$+$6N_2$+36	$3N_1$+$3N_2$+4	$4N_1$+13	3	N_2
BPS	N_1M+$2N_1$M	$2N_1$M-M+3	M+1	0	N_1M+N_1
BPS+MLE	N_1M+$2N_1$M+N_2	$2N_1$M-M+N_2+2	M+1	1	N_1M+N_2

TABLE II
COMPUTATIONAL COMPLEXITY FOR VARIOUS CPE ALGORITHMS

linewidth of almost 1.2 MHz hence making it possible to operate the optical 64-QAM system with current commercial tunable lasers.

REFERENCES

[1] S. Zhang, P.-Y. Kam, C. Yu, and J. Chen, "Decision-aided carrier phase estimation for coherent optical communications," *Lightwave Technology, Journal of*, vol. 28, no. 11, pp. 1597 –1607, june1, 2010.

[2] A. Gnauck, P. Winzer, S. Chandrasekhar, X. Liu, B. Zhu, and D. Peckham, "10 x 224-Gb/s WDM transmission of 28-Gbaud PDM 16-QAM on a 50-GHz grid over 1,200 km of fiber," in *Proc. of OFC/NFOEC 2010, San Diego, paper PDPB8*, March 2010.

[3] K. Kikuchi, "Analyses of wavelength- and polarization-division multiplexed transmission characteristics of optical quadrature-amplitude-modulation signals," *Opt. Express*, vol. 19, no. 19, pp. 17 985–17 995, Sep 2011.

[4] X. Zhou and J. Yu, "200-Gb/s PDM-16QAM generation using a new synthesizing method," in *Proc. of ECOC 2009, Vienna (Austria), paper 10.3.5*, September 2009.

[5] A. Sano, T. Kobayashi, K. Ishihara, H. Masuda, S. Yamamoto, K. Mori, E. Yamazaki, E. Yoshida, Y. Miyamoto, T. Yamada, and H. Yamazaki, "240-Gb/s polarization-multiplexed 64-QAM modulation and blind detection using PLC-LN hybrid integrated modulator and digital coherent receiver," in *Proc. of ECOC 2009, Vienna (Austria), paper PD2.2*, September 2009.

[6] E. Ip and J. M. Kahn, "Feedforward carrier recovery for coherent optical communications," *J. Lightwave Technol.*, vol. 25, no. 9, pp. 2675–2692, Sep 2007.

[7] L. Kazovsky, "Impact of laser phase noise on optical heterodyne communication systems," *Journal of Optical Communications.*, vol. 7, no. 2, pp. 41–80, june 1986.

[8] ——, "Performance analysis and laser linewidth requirements for optical PSK heterodyne communications systems," vol. 4, no. 4, apr 1986, pp. 415 – 425.

[9] R. Slavic, F. Parmigiani, J. Kakande, and et al., "All-optical phase and amplitude regenerator for next-generation telecommunications systems," *Nature Photonics*, vol. 4, no. 10, pp. 690–695, 2010.

[10] A. Tarighat, R. Hsu, A. Sayed, and B. Jalali, "Digital adaptive phase noise reduction in coherent optical links," *Lightwave Technology, Journal of*, vol. 24, no. 3, pp. 1269 –1276, march 2006.

[11] M. Seimetz, "Laser linewidth limitations for optical systems with high-order modulation employing feed forward digital carrier phase estimation," in *Proc. of OFC/NFOEC 2008, San Diego, paper OTuM2*, Feb. 2008.

[12] S. M. Bilal, A. Carena, C. Fludger, and G. Bosco., "Dual stage CPE for 64-QAM optical systems based on a modified QPSK-partitioning algorithm," *Photonics Technology Letters, IEEE*, vol. 26, no. 3, pp. 267–270, february 1, 2014.

[13] S. M. Bilal, C. Fludger, and G. Bosco., "Multi-stage CPE algorithms for 64-QAM constellations," in *Proc. of OFC/NFOEC 2014, San Francisco, paper M2A.8*, March 2014.

[14] S. M. Bilal and G. Bosco, "Dual stage carrier phase estimation for 16-QAM systems based on a modified QPSK-partitioning algorithm," in *Proc. of ICTON 2013, Cartagena (Spain), paper We.D1.2*, June 2013.

[15] S. M. Bilal, K. P. Zhong, J. Cheng, A. P. T. Lau, G. Bosco, and C. Lu, "Performance and complexity comparison of carrier phase estimation algorithms for DP-64-QAM optical signals," in *Proc. of ECOC 2014, Cannes (France), paper P.3.11*, September 2014.

[16] S. M. Bilal, G. Bosco, A. P. T. Lau, and C. Lu, "Linewidth-tolerant feed-forward dual-stage CPE algorithm based on 64-QAM constellation partitioning," in *Proc. of ECOC 2014, Cannes (France), paper P.3.24*, September 2014.

[17] T. Pfau, S. Hoffmann, and R. Noe, "Hardware-efficient coherent digital receiver concept with feedforward carrier recovery for M-QAM constellations," *Lightwave Technology, Journal of*, vol. 27, no. 8, pp. 989 –999, april15, 2009.

[18] S. K. Oh and S. Stapleton, "Blind phase recovery using finite alphabet properties in digital communications," *Electronics Letters*, vol. 33, no. 3, pp. 175–176, 1997.

[19] F. Rice, B. Cowley, B. Moran, and M. Rice, "Cramer-rao lower bounds for QAM phase and frequency estimation," *Communications, IEEE Transactions on*, vol. 49, no. 9, pp. 1582–1591, 2001.

[20] Q. Zhuge, C. Chen, and D. V. Plant, "Low computation complexity two-stage feedforward carrier recovery algorithm for M-QAM," in *Optical Fiber Communication Conference/National Fiber Optic Engineers Conference 2011*. Optical Society of America, 2011, p. OMJ5.

[21] J. Li, L. Li, Z. Tao, T. Hoshida, and J. Rasmussen, "Laser-linewidth-tolerant feed-forward carrier phase estimator with reduced complexity for QAM," *Lightwave Technology, Journal of*, vol. 29, no. 16, pp. 2358–2364, 2011.

[22] A. Viterbi, "Nonlinear estimation of PSK-modulated carrier phase with application to burst digital transmission," *Information Theory, IEEE Transactions on*, vol. 29, no. 4, pp. 543–551, 1983.

[23] K. Zhong, J. H. Ke, Y. Gao, and J. C. Cartledge, "Linewidth-tolerant and low-complexity two-stage carrier phase estimation based on modified QPSK partitioning for dual-polarization 16-QAM systems," *J. Lightwave Technol.*, vol. 31, no. 1, pp. 50–57, Jan 2013.

[24] S. M. Bilal, C. Fludger, V. Curri, and G. Bosco., "Multi-stage CPE algorithms for phase noise mitigation in 64-QAM optical systems," *J. Lightwave Technol.*, vol. 32, no. 17, pp. 2973–2980, September 2014.

[25] S. M. Bilal, G. Bosco., P. Poggiolini, and C. Fludger, "Low-complexity linewidth-tolerant carrier phase estimation for 64-QAM systems based on constellation transformation," in *Proc. of ECOC 2013, London (United Kingdom), paper P.3.7*, September 2013.

[26] X. Zhou, "An improved feed-forward carrier recovery algorithm for coherent receivers with M-QAM modulation format," *Photonics Technology Letters, IEEE*, vol. 22, no. 14, pp. 1051 –1053, july15, 2010.

[27] Y. Miyata, K. Sugihara, W. Matsumoto, K. Onohara, T. Sugihara, K. Kubo, H. Yoshida, and T. Mizuochi, "A triple-concatenated FEC using soft-decision decoding for 100 Gb/s optical transmission," in *Proc. of OFC/NFOEC 2010, San Diego, paper OThL3*, March 2010.

[28] J.-K. Hwang, Y.-L. Chiu, and C.-S. Liao, "Angle differential-QAM scheme for resolving phase ambiguity in continuous transmission system," *Int. J. Commun. Syst.*, vol. 21, no. 6, pp. 631–641, 2008.